# Pair approximation of the stochastic susceptible-infected-recovered-susceptible epidemic model on the hypercubic lattice

Jaewook Joo

*Department of Physics, Rutgers University, New Brunswick, New Jersey 08854, USA*

Joel L. Lebowitz

*Department of Mathematics and Physics, Rutgers University, New Brunswick, New Jersey 08854, USA*

(Received 10 May 2004; published 23 September 2004)

We investigate the time evolution and steady states of the stochastic susceptible-infected-recovered-susceptible (SIRS) epidemic model on one- and two-dimensional lattices. We compare the behavior of this system, obtained from computer simulations, with those obtained from the mean-field approximation (MFA) and pair approximation (PA). The former (latter) approximates higher-order moments in terms of first- (second-) order ones. We find that the PA gives consistently better results than the MFA. In one dimension, the improvement is even qualitative.

## I. INTRODUCTION

The mathematical modeling of the spread of epidemics is a subject of continuing theoretical and practical interest [1,2]. This is enhanced by the fact that the same or similar models are used for describing other phenomena such as plant and animal dispersal, and successional dynamics in ecology [3,4].

The level of description provided by a model can be purely macroscopic and deterministic or individual and stochastic [5]. In the first case, one uses (partial-) differential equations to describe the time evolution of different sub-populations, e.g., susceptible, infectious, and recovered. In the second case, one typically uses stochastic dynamics on a lattice (or more general graphs) where the variables at each node represent the state of an individual or a small spatial region. The time evolution of these variables is stochastic, e.g., an infected individual at site $i$ has a certain probability per unit time (rate) $\lambda$ to infect a susceptible individual at a neighboring site $j$. These systems fall into the category of what mathematicians call interacting particle systems [6,7] and physicists call stochastic lattice gases [8]—systems of great interest also in the study of equilibrium phase transitions, phase segregation kinetics, etc., fields very different from epidemiology and ecology.

The connection between these modes of description and various intermediate ones has been investigated extensively in recent years, e.g., see [5,9–13]. Mathematically, this involves the use of the so-called hydrodynamical scaling limit. This uses a rigorous separation of space and time scales to derive deterministic macroscopic equations from the microscopic dynamics of stochastic lattice systems. Other approaches are based on more heuristic methods such as the mean-field approximation (MFA) and improvement thereof [14–25].

The present work falls in the latter category. We apply a pair approximation (PA) scheme to a microscopic stochastic epidemic model in which individuals recovered from an infection enjoy a period of immunity before again becoming susceptible at a rate $\gamma$: the SIRS model. The PA approximation was used by Levin and Durrett [16] for the simpler susceptible-infected-susceptible (SIS) model where recovered individuals immediately become susceptible again. They compared the results of the PA and MFA with those of the stochastic SIS model and found that the PA gave a quantitative improvement over the MFA. Here we consider the general SIRS model. We obtain the behavior of the stochastic model from extensive computer simulations. We then solve the PA and MFA models analytically for the stationary state and numerically for the time-dependent case. We find that the PA gives considerably better agreement with the simulations than the MFA both for the time evolution and for the steady state. For the latter, the PA reproduces the qualitative difference between the one- and higher-dimensional phase diagram of this model found in Refs. [26–29]. This is reminiscent of the relation between the MFA and the Bethe-Peierls approximation (which the PA closely resembles) for equilibrium lattice systems [30].

## II. THE STOCHASTIC SIRS MODEL

We first recall the stochastic lattice model of the SIRS epidemic process [31]. A site $x$ of a $d$-dimensional lattice can be occupied by an individual in a state of $S$ (healthy and susceptible), $I$ (infected), or $R$ (recovered, i.e., healthy and immune). The system evolves according to the following transition rates:

$$S \rightarrow I \quad \text{at rate} \quad \lambda n(x),$$

$$I \rightarrow R \quad \text{at rate} \quad \delta,$$

$$R \rightarrow S \quad \text{at rate} \quad \gamma, \tag{1}$$

where $n(x)$ is the number of infected (nearest) neighbors of $x$, $\lambda$ is the infection rate, $\delta$ is the recovery rate, and $\gamma$ is the rate at which immunization ceases. The limit $\gamma \rightarrow \infty$ corresponds to the case where a recovered site passes instanta-

neously through the state $R$; this is the SIS model, also known as the contact process. We shall choose time units in which $\delta = 1$.

One can obtain some rigorous qualitative information about this and related models via probabilistic approaches such as those used in interacting particle systems [26–29]. Of particular interest is the behavior of the stationary state on an infinite lattice which is a good approximation for the quasi-steady-state behavior of large systems, see Appendix E. This information is encoded in the phase diagram of the stationary state, which depends on the infection rate $\lambda$, the recovery rate $\gamma$, and the topology of the lattice. For small $\lambda$, the only stationary state is one in which all sites are in the susceptible (disease-free) state while for large $\lambda$ there is (for the infinite system) also a stationary state containing a nonzero fraction of $I$ and $R$ individuals.

The critical infection rate $\lambda_c(\gamma)$ is defined as the smallest value of $\lambda$, for a given $\gamma$, above which the infection can persist forever. For the SIS or contact process ($\gamma = \infty$), the critical infection value is known with high accuracy, $\lambda_c(\infty) \simeq 1.6489$ in $d=1$ and $\lambda_c(\infty) \simeq 0.4122$ in $d=2$ [6,8]. Considerably less is known about the phase diagram of the SIRS model. Interestingly, there is a qualitative difference in the behavior of $\lambda_c(\gamma)$ in one and in higher dimensions when $\gamma \to 0$. It has been shown that $\lim_{\gamma \to 0} \lambda_c(\gamma) = \lambda_c(0)$ is finite when $d \geq 2$ while $\lambda_c(0) = \infty$ when $d=1$ [26–29].

To go beyond qualitative results, we need to carry out a simulation or make some approximations. This is the subject of the rest of the paper.

### III. THE PAIR APPROXIMATION

The time evolution of the single-site probabilities in the stochastic SIRS epidemic process can be written in the following form:

$$\frac{dP_t(S_x)}{dt} = -\lambda \sum_{y \in \mathcal{N}(x)} P_t(S_x, I_y) + \gamma P_t(R_x), \qquad (2a)$$

$$\frac{dP_t(I_x)}{dt} = \lambda \sum_{y \in \mathcal{N}(x)} P_t(S_x, I_y) - P_t(I_x), \qquad (2b)$$

$$\frac{dP_t(R_x)}{dt} = P_t(I_x) - \gamma P_t(R_x). \qquad (2c)$$

Here $\mathcal{N}(x)$ is the neighborhood (nearest-neighbor sites) of a site $x$, $P_t(\alpha_x)$ is the probability of having a state $\alpha$ at site $x$ at time $t$, and $P_t(\alpha_x, \beta_y)$ is the joint probability to have state $\alpha$ at site $x$ and state $\beta$ at site $y$, at time $t$. We always have $P_t(S_x) + P_t(I_x) + P_t(R_x) = 1$.

Equations (2a)–(2c) are, as is usual for moment equations, not a closed system. One can extend them by including equations for the time evolution of $P_t(S_x, I_y)$, which in turn involve higher moments of the spatial correlations. This leads to an infinite hierarchy. To solve such a hierarchy, one usually resorts to some approximation scheme which expresses the higher-order moments in terms of the lower-order ones and truncates the equations at some point; this is referred to

as the moment closure method [14–25]. Both the MFA and PA are such schemes. In the MFA, Eqs. (2a)–(2c) are closed by assuming that $P_t(S_x, I_y) = P_t(S_x) P_t(I_y)$, i.e., it neglects correlations between different sites. This leads to a pair of coupled equations which have been studied in [31]. In the PA scheme, $P_t(\alpha_x)$ and $P_t(\alpha_x, \beta_y)$ are kept as unknowns while the higher-order moments are expressed, via some appropriate approximation, in terms of these quantities.

To carry out the PA, we complement Eq. (2) by equations for the second moments $P_t(\alpha_x, \beta_y)$ for nearest-neighbor sites $x$ and $y$ based on the transition rule that we have described in Eq. (1). These are

$$\frac{dP_t(S_x, I_y)}{dt} = \gamma P_t(R_x, I_y) - (\lambda + 1) P_t(S_x, I_y)$$

$$+ \sum_{w \in \mathcal{N}^x(y)} \lambda P_t(S_x, S_y, I_w) - \sum_{w \in \mathcal{N}^y(x)} \lambda P_t(I_w, S_x, I_y),$$

$$\qquad (3a)$$

$$\frac{dP_t(S_x, R_y)}{dt} = P_t(S_x, I_y) + \gamma P_t(R_x, R_y)$$

$$- \gamma P_t(S_x, R_y) - \sum_{w \in \mathcal{N}^y(x)} \lambda P_t(I_w, S_x, R_y), \quad (3b)$$

$$\frac{dP_t(R_x, I_y)}{dt} = -(\gamma + 1) P_t(R_x, I_y) + P_t(I_x, I_y)$$

$$+ \sum_{w \in \mathcal{N}^x(y)} \lambda P_t(R_x, S_y, I_w), \qquad (3c)$$

where $\mathcal{N}^x(y)$ is the set of nearest-neighbor sites of $y$ excluding the site $x$. $P_t(\alpha_x, \beta_y, \chi_w)$ is the joint probability to have state $\alpha$ at site $x$, state $\beta$ at site $y$, and state $\chi$ at site $w$ at time $t$. For a derivation of Eq. (3), see Appendix A.

To close the system (2) and (3) and derive a set of autonomous equations for $P_t(\alpha_x)$ and $P_t(\alpha_x, \beta_y)$, we approximate the triad joint probability $P_t(\alpha_x, \beta_y, \chi_w)$ for $x$ and $w$ nearest neighbors of $y$, by the product of two pair probabilities $P_t(\alpha_x, \beta_y)$ and $P_t(\beta_y, \chi_w)$ divided by the probability $P_t(\beta_y)$ [14–18], i.e., we set

$$P_t(\alpha_x, \beta_y, \chi_w) = \frac{P_t(\alpha_x, \beta_y) P_t(\beta_y, \chi_w)}{P_t(\beta_y)}. \qquad (4)$$

Note that we have made use here of the structure of the hypercubic lattice. In such lattices, three adjacent sites—$x, y, w$—cannot form a triangle but form only linear chains. This is not so in other lattices, e.g., the triangular lattice, where other configurations need also be considered.

While there are other choices for a PA, the approximation in Eq. (4) allows one to get the steady-state solutions analytically. With other pair approximations [25], one has to solve the resulting differential equations numerically, making it impossible to obtain analytic expressions for the critical curve.

To actually carry out computations with the PA, we will assume from now on that our system is spatially uniform. The site $x$, in Eqs. (2) and (3), can now be chosen to be the

origin. We also define $P_t(S,I)=(1/z)\Sigma_{y\in\mathcal{N}(x)}\,P_t(S_x,I_y)$ and $P_t(\alpha,\beta,\chi)=[1/(z-1)]\Sigma_{w\in\mathcal{N}^x(y)}\,P_t(\alpha_x,\beta_y,\chi_w)$, where $z=2d$ is the number of nearest neighbors of a site in the $d$-dimensional cubic lattice. The truncated equations for the PA-SIRS can now be written, by using the exact Eqs. (2) and (3) and the approximate Eq. (4), as a closed set of five coupled equations,

$$\frac{dP_t(I)}{dt}=z\lambda P_t(S,I)-P_t(I), \tag{5a}$$

$$\frac{dP_t(R)}{dt}=P_t(I)-\gamma P_t(R), \tag{5b}$$

$$\frac{dP_t(S,R)}{dt}=P_t(S,I)+\gamma[P_t(R)-P_t(R,I)-2P_t(S,R)]$$
$$-\frac{(z-1)\lambda P_t(S,I)P_t(S,R)}{1-P_t(R)-P_t(I)}, \tag{5c}$$

$$\frac{dP_t(R,I)}{dt}=-(2+\gamma)P_t(R,I)+P_t(I)-P_t(S,I)$$
$$+\frac{(z-1)\lambda P_t(S,I)P_t(S,R)}{1-P_t(R)-P_t(I)}, \tag{5d}$$

$$\frac{dP_t(S,I)}{dt}=\gamma P_t(R,I)-(\lambda+1)P_t(S,I)$$
$$+\frac{(z-1)\lambda P_t(S,I)}{1-P_t(I)-P_t(R)}$$
$$\times[1-P_t(R)-P_t(I)-P_t(S,R)-2P_t(S,I)]. \tag{5e}$$

Note that we always have $P_t(\alpha)=P_t(\alpha,S)+P_t(\alpha,I)+P_t(\alpha,R)$, which determines $P_t(I,I)$ and $P_t(S,S)$.

In the limit $\gamma\to\infty$, $P_t(R)$ and $P_t(R,\alpha)$ as well as their time derivatives will go to zero. This yields $\gamma P_t(R)=P_t(I)$ and $\gamma P_t(R,I)=P_t(I)-P_t(S,I)$ [31]. In this limit, Eq. (5) reduces to the PA equations of the SIS considered in [16],

$$\frac{dP_t(I)}{dt}=z\lambda P_t(S,I)-P_t(I), \tag{6a}$$

$$\frac{dP_t(S,I)}{dt}=P_t(I)-(\lambda+2)P_t(S,I)$$
$$+\frac{(z-1)\lambda P_t(S,I)}{1-P_t(I)}[1-P_t(I)-2P_t(S,I)]. \tag{6b}$$

As already noted, the MFA approximates the joint probability $P_t(S,I)$ in Eq. (5a) by the product $P_t(S,I)=P_t(S)P_t(I)$. This leads to the closed set of the MFA of equations for the SIRS [31],

$$\frac{dP_t(S)}{dt}=-z\lambda P_t(S)P_t(I)+\gamma P_t(R), \tag{7a}$$

$$\frac{dP_t(I)}{dt}=z\lambda P_t(S)P_t(I)-P_t(I), \tag{7b}$$

$$\frac{dP_t(R)}{dt}=P_t(I)-\gamma P_t(R). \tag{7c}$$

For $\gamma\to\infty$, $\gamma P_t(R)\to P_t(I)$ and $P_t(S)\to1-P_t(I)$. Equation (7) then reduces to the MFA for the SIS.

## IV. STATIONARY SOLUTIONS OF THE PA-SIRS MODEL

Let us first consider the steady-state solutions of the PA-SIS obtained by setting the left-hand side of Eq. (6) equal to zero [16]. This gives for the critical value of the PA-SIS epidemic process $\lambda_c(\infty)=1/(z-1)$. For $\lambda\le\lambda_c(\infty)$, both $P_t(I)$ and $P_t(S,I)\to0$ as $t\to\infty$ for all initial states. When $\lambda>\lambda_c(\infty)$, there is, in addition to the disease-free state corresponding to $P(I)=0$, also a stationary state consisting of a finite fraction of infected individuals,

$$\bar{P}(S,I)=\bar{P}(I)/(z\lambda), \tag{8a}$$

$$\bar{P}(I)=\frac{z[(z-1)\lambda-1]}{z(z-1)\lambda-1}. \tag{8b}$$

It is these nonzero steady states which are approached as $t\to\infty$ when starting from any initial state with $P_0(I)>0$.

The steady-state solutions of the PA-SIRS system are obtained by setting the left-hand side of Eq. (5) equal to zero. Setting $x=\bar{P}(I)$, this yields

$$\bar{P}(R)=x/\gamma, \tag{9a}$$

$$\bar{P}(S,I)=x/(z\lambda), \tag{9b}$$

$$\bar{P}(S,R)=\frac{x\left(\dfrac{1}{z\lambda}+\dfrac{1}{\gamma+1}\right)}{\gamma\left(1+\dfrac{1}{\gamma+1}+\dfrac{(z-1)x}{z[\gamma-(1+\gamma)x]}\right)}, \tag{9c}$$

$$\bar{P}(R,I)=\frac{x-\gamma\bar{P}(S,R)}{\gamma+1}$$
$$=\frac{x}{\gamma+1}\left(1-\frac{\dfrac{1}{z\lambda}+\dfrac{1}{\gamma+1}}{1+\dfrac{1}{\gamma+1}+\dfrac{(z-1)x}{z[\gamma-(\gamma+1)x]}}\right), \tag{9d}$$

where $\bar{P}(\alpha,\beta)$ are the approximate probabilities for having states $\alpha$ and $\beta$ on neighboring sites. After further simplifications, we find that $x$ has to satisfy the cubic equation

$$x(a_1x^2+a_2x+a_3)=0. \tag{10}$$

Both the derivation of Eq. (10) and the explicit expressions for $a_1$, $a_2$, and $a_3$ as functions of $\lambda$ and $\gamma$ are given in Appendix B.
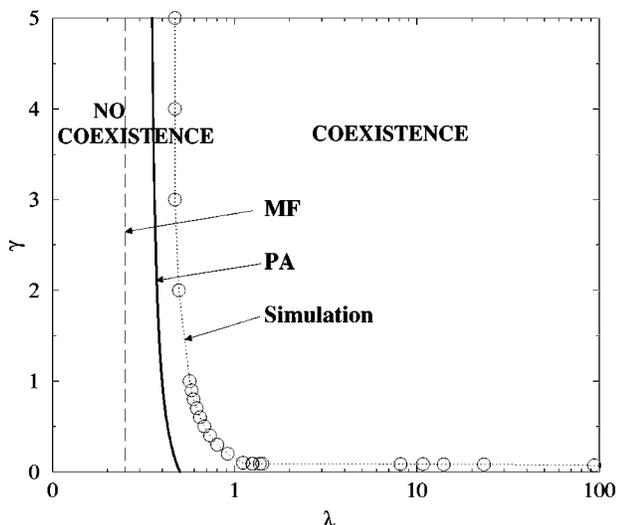
FIG. 1. Phase diagram of the SIRS process in two dimensions. The coexistence phase of *S-I-R* and the no-coexistence phase are separated by the critical curve from the simulation (open circles with dotted line to guide the eye), the PA (thick solid line), and the MFA (long dashed line). The critical curve is obtained on a periodic square lattice of different sizes $N$ from simulations extrapolated to an infinite system: $N=50^2, 70^2, 100^2, 150^2, 200^2$.

The root $x=0$ corresponds to the all healthy steady state, which is always a solution. The critical curve $\lambda_c(\gamma)$ is determined by the existence of a root of Eq. (10) such that $x$ and all other stationary probabilities are strictly positive. It turns out that this strictly positive root is unique. Thus when $\lambda \leqslant \lambda_c(\gamma)$, $x=0$ is the only steady-state solution. For $\lambda > \lambda_c(\gamma)$, there is also a steady state in which the infection is endemic: $\bar{P}(I) = \gamma\bar{P}(R) = x$ and $\bar{P}(S) = 1-(1+1/\gamma)x$, see Appendix B.

The critical curve $\lambda_c(\gamma)$ is obtained in Appendix B. It is given by the equation

$$\lambda_c(\gamma) = \frac{\gamma+1}{2d-2+(2d-1)\gamma}, \quad d=1,2,3,\dots. \quad (11)$$

As $\gamma \to \infty$, $\lambda_c(\infty) = (2d-1)^{-1}$, the critical point of the PA-SIS epidemic process. On the other hand, as $\gamma$ approaches zero, the critical curve shows different behavior depending on the dimension of the lattice: $\lambda_c(0)$ diverges to infinity for $d=1$, while $\lambda_c(0)$ is finite for $d \geqslant 2$. The PA thus reproduces the qualitative difference between the one- and higher-dimensional phase diagram of the SIRS model found in Refs. [26–29].

The MFA, Eq. (7), yields the mean-field critical value, $\lambda_c^{MF} = 1/z$ independent of $\gamma$. In the coexistence region $\lambda > \lambda_c^{MF}$, the mean-field stationary states are $\bar{P}(I) = \gamma\bar{P}(R)$ $= [\gamma(\lambda z-1)]/[\lambda z(\gamma+1)]$ and $\bar{P}(S) = 1/z\lambda$.

Both the steady state and critical value of the MFA and PA fail to correctly represent the results of the stochastic SIRS process for small $\gamma$; see Figs. 1 and 2. Note in particular that $\bar{P}(S)$ of the stochastic SIRS process is considerably larger than that of the MFA or PA for large $\lambda$ and small $\gamma$.
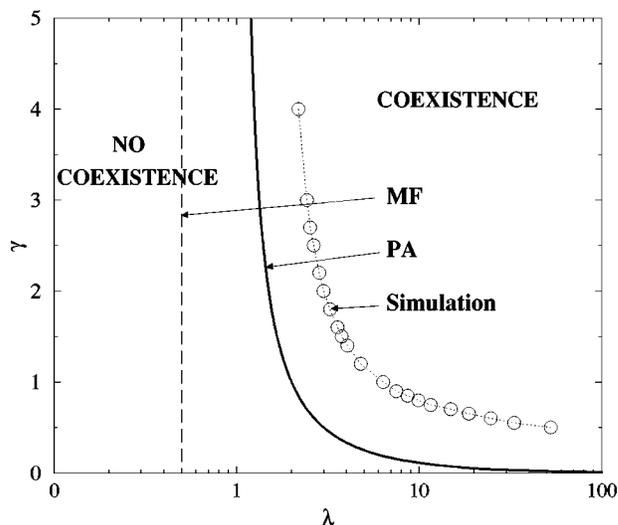


FIG. 2. Phase diagram of the SIRS process in one dimension. The critical curve from numerical simulations of a ring lattice of different sizes $N$ is extrapolated to an infinite system: $N = 5000, 7000, 10\,000, 15\,000$. The same symbols are used as in Fig. 1.

This is due to the fact that the susceptible sites can be surrounded by recovered ones and thus protected from contacting infected ones in the stochastic case.

## V. COMPARISON OF THE STOCHASTIC, PA, AND MFA STEADY STATES

We compare in Figs. 3–6 the steady-state values of $\bar{P}(\alpha)$ and $\bar{P}(\alpha,\beta)$ obtained from the MFA and PA with the results
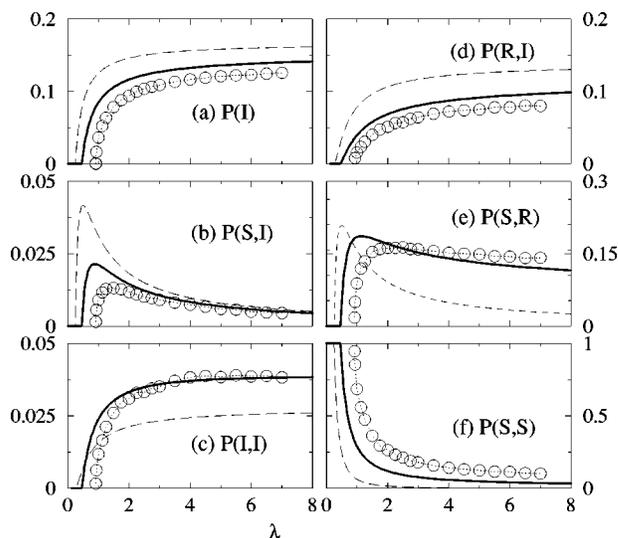


FIG. 3. First- and second-order moments of the steady-state SIRS in two dimensions at $\gamma=0.2$. The steady-state values of the density of infection in (a) and the second moments in (b)–(f) are drawn from the numerical simulation (open circle with dotted line to guide the eye), the PA (thick solid line), and the MFA (long-dashed line). For the numerical simulation, we used a system of size $N = 100^2$.
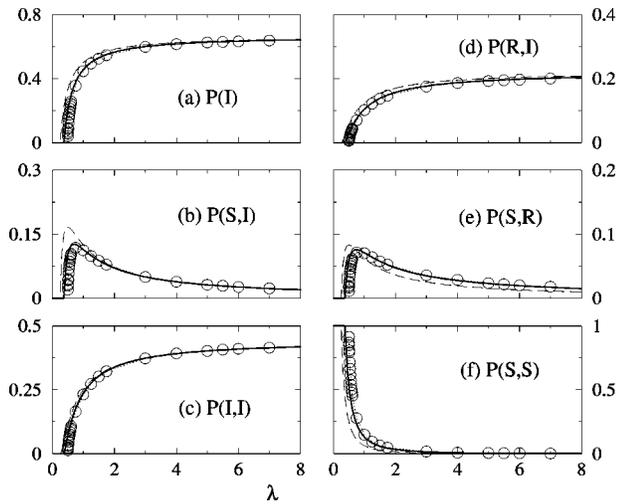
FIG. 4. First- and second-order moments of the steady-state SIRS in two dimension at $\gamma=2$. The same symbols are used as in Fig. 3.



FIG. 6. First- and second-order moments of the steady-state SIRS process in one dimension at $\gamma=4$. The same symbols are used as in Fig. 3.

from the stochastic SIRS process as a function of $\lambda$ at fixed values of $\gamma$. Clearly the PA gives results closer to those obtained from the stochastic model. For the methods used to obtain the steady-state results from the numerical simulation, see Appendix E.

Figures 3 and 5 show that both the MFA and PA overestimate $\bar{P}(I)$ as well as $\bar{P}(\alpha,I)$, $\alpha=S,R$. This is due to the strong tendency of infected sites in the stochastic model to cluster into localized islands, reducing the contacts between $S$ and $I$. This is partially taken into account by the PA as seen by the behavior of $\bar{P}(S,I)$ and $\bar{P}(I,I)$ in Figs. 3 and 5. This clustering effect is also observed in the stochastic SIS process [16]. It is more pronounced in one dimension.

Note that $\bar{P}(S,I)$ becomes zero both at $\lambda<\lambda_c(\gamma)$ when $\bar{P}(I)=0$, and at $\lambda=\infty$ when $\bar{P}(S)=0$, reaching a peak at a positive value of $\lambda$ which depends on $\gamma$. For large values of
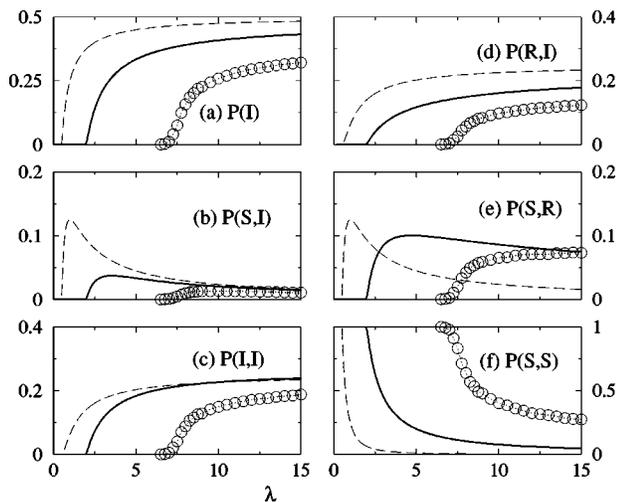


FIG. 5. First- and second-order moments of the steady-state SIRS process in one dimension at $\gamma=1$. The same symbols are used as in Fig. 3.
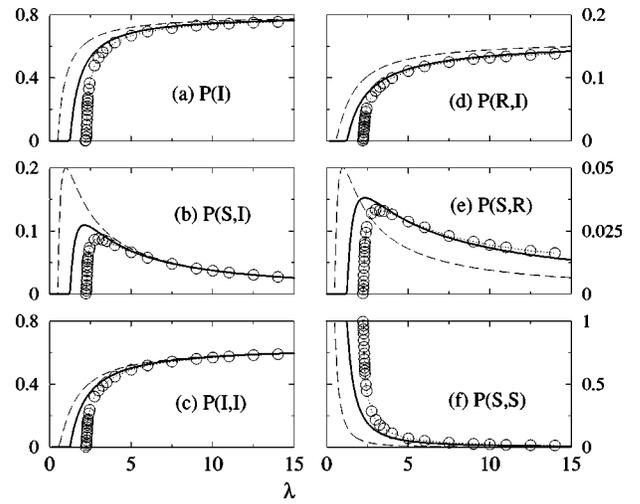
$\gamma$, the steady-state values of $\bar{P}(\alpha)$ and $\bar{P}(\alpha,\beta)$ obtained from the PA or the MFA agree well with the numerical simulation, away from the critical $\lambda_c(\gamma)$. Moreover, the PA yields steady-state curves remarkably similar to those from the numerical simulation; see Figs. 4–6.

## VI. LINEAR STABILITY ANALYSIS OF THE PAIR APPROXIMATION

To study the stability of the stationary PA state, Eq. (5) is linearized about the steady-state values [31]; see Appendix C. This leads to the study of the roots of the characteristic fifth-order polynomial $P_5(\xi)$, obtained from $|A-\xi I|=0$, where $A$ is the Jacobian of the linearized PA-SIRS system. If Re $\xi<0$, the solution of the linearized equation is stable, i.e., a small perturbation around the steady state will decay back to the steady state. We used the Routh-Hurwitz conditions [31] to obtain the sign of the real part of eigenvalues of the Jacobian. As expected, the positive steady-state solution is stable for $\lambda>\lambda_c(\gamma)$. The zero steady-state solution is stable for $\lambda\leq\lambda_c(\gamma)$ and unstable for $\lambda>\lambda_c(\gamma)$.

The eigenvalues of $P_5(\xi)$ have nonzero imaginary parts in some regions of the parameter space. In such regions, the PA-SIRS system in Eq. (5) will converge to the steady state in a damped oscillatory manner. Such oscillations are seen in Figs. 7 and 8.

## VII. TIME-DEPENDENT BEHAVIOR

To study the time evolution of an epidemic following an initial infection of a healthy population, we performed dynamical Monte Carlo simulations [33] as well as solutions of Eqs. (5) and (7). For the stochastic evolution, we started with infected sites placed either randomly or in a cluster and followed the time evolution averaged over $10^3$ realizations of the SIRS process. To obtain the time evolution of the MFA and PA, we solved Eqs. (7) and (5) numerically by using a
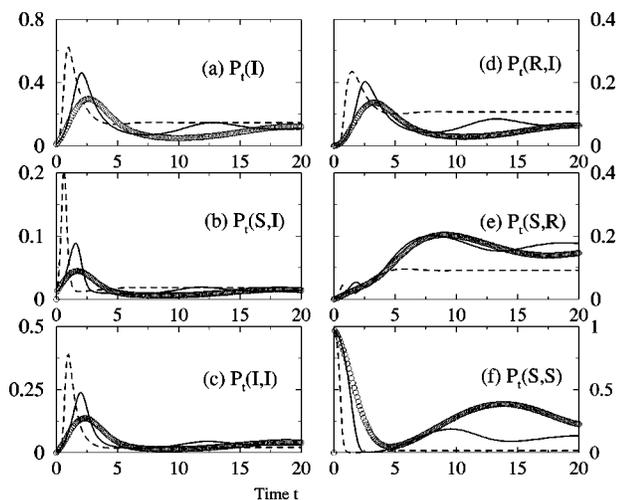
FIG. 7. Time evolution of the first- and the second-order moments of the SIRS process in two dimensions. All subgraphs are from numerical simulations (open circles), the PA (solid line), and the MFA (dashed line) at $\gamma = 0.2$ and $\lambda = 2$. A periodic square lattice of $N = 10^4$ sites is used in the numerical simulations averaged over $10^3 - 10^4$ realizations starting with random initial distribution with 1% of infected sites.

fourth-order Runge-Kutta method. We plot the results in Figs. 7 and 8.

To set the unit of time of the simulation, we started with a fully infected state, $P_0(I) = 1$ and $\lambda = 0$, and obtained the exponentially decaying pattern of $P_t(I)$. We then set the slope (death rate) of the graph, $\log P_t(I)$ versus $t$, from the numerical simulation equal to those from the MFA and PA.
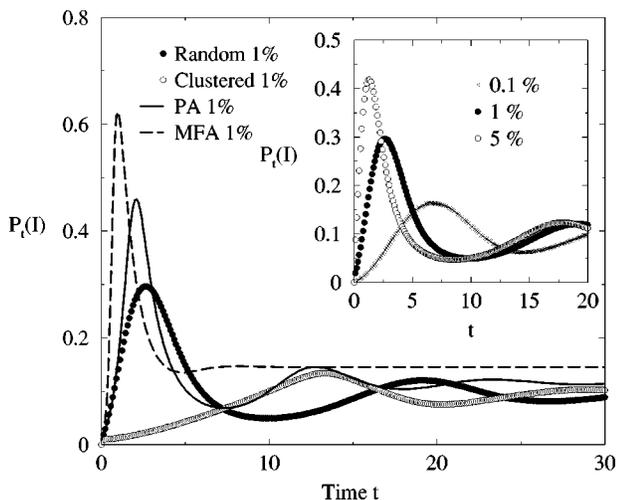


FIG. 8. Time evolution of a fraction of infected sites of the SIRS process in two dimensions at $\gamma = 0.2$ and $\lambda = 2$. A periodic square lattice of $N = 100^2$ is used in numerical simulation averaged over $10^3 - 10^4$ realizations. Main: Simulation starts with 1% of infected sites placed either randomly (filled circles) or in a single cluster (open circles) on a lattice. Both the PA and MFA take an initial value 0.01 for $P_0(I)$. Inset: Simulation starts with different fractions of infected sites randomly placed in a lattice: 0.1%, 1%, and 5% of the system.

Starting with a small value of $P_0(I)$, $P_t(I)$ displays an initial "exponential" growth in both the MFA and PA. Similar growth patterns are observed in all $P_t(\alpha, I)$, $\alpha = S, I, R$. This is explained by the initially abundantly available susceptible population. Once the susceptible population is reduced, the infected population reaches a maximum and then decreases to the steady-state endemic level. Note the damped oscillatory pattern in Figs. 7 and 8 for this choice of the parameters $(\lambda, \gamma)$.

The numerical simulation of the stochastic time evolution does not show the pronounced growth patterns of the PA and MFA when the initial fraction of infected sites is small, as seen in Fig. 8. The formation of clusters of infected sites makes the infected population grow more slowly in the stochastic model. When the initial fraction of infected population increases to more than 1%, the stochastic model shows significant change in its growth pattern, becoming similar to the PA and MFA. If, however, the same fraction of infected sites are initially placed in a single cluster, the stochastic epidemic process exhibits slower growth patterns, similar to those starting with a small fraction of initially infected sites. These studies confirm that the clustering of infected sites in the stochastic model reduces both the speed of growth and the maximum fraction of infected sites. In realistic situations, the population is not well mixed so we would expect growth patterns more similar to that of the stochastic epidemic model, starting with a fraction of infected sites initially placed in a single cluster.

## VIII. SUMMARY

We investigated the stochastic SIRS epidemic process and compared the results with those obtained from the deterministic MFA and PA. These approximations close the hierarchy of dynamical equations by expressing the higher-order moments in terms of the lower-order ones. The PA is found to improve over the MFA both for the stationary and for the time-dependent states. The time evolution of the system shows damped oscillatory behavior in some parameter ranges.

*Note added in proof.* Recently, we became aware of the work by Kobayashi, Sato, and Konno [34] where the stationary state for the SIRS model in the square lattice was investigated by using Monte Carlo simulation and pair approximation. Our results agree with theirs. We thank N. Konno for bringing this to our attention.

## ACKNOWLEDGMENTS

## APPENDIX A: DERIVATION OF DIFFERENTIAL EQUATION FOR $P_t(S_x, I_y)$

Equation (3a) is derived by considering all transitions leaving or entering the pair configuration $(S_x, I_y)$. We list them as follows. A pair $(R_x, I_y)$ changes to a pair $(S_x, I_y)$ with

a rate $\gamma$. A pair $(S_x, I_y)$ changes to a pair $(I_x, I_y)$ with a rate $\lambda$ and also changes to a pair $(S_x, R_y)$ with a rate 1. A triad configuration $(S_x, S_y, I_w)$ transits to a triad $(S_x, I_y, I_w)$ with a rate $\lambda$ such that a pair configuration $(S_x, S_y)$ is changed to $(S_x, I_y)$. A triad $(I_w, S_x, I_y)$ changes to a triad $(I_w, I_x, I_y)$ with a rate $\lambda$. The equations for $P_t(S_x, R_y)$ and $P_t(R_x, I_y)$ in Eq. (3) can be obtained in a similar way. The relation $P_t(\alpha_x) = P_t(\alpha_x, \alpha_y) + P_t(\alpha_x, \beta_y) + P_t(\alpha_x, \chi_y)$ can be used to obtain the other joint probabilities $P_t(\alpha_x, \beta_y)$ which are not shown in Eq. (3).

## APPENDIX B: DERIVATION OF EQ. (10)

The steady states in Eq. (9) are obtained by setting the lhs of Eqs. (5a)–(5d) equal to zero. In addition, we set Eq. (5e) equal to zero and replace a single site and joint probabilities with the steady states in Eq. (9). After simplifications, we obtain Eq. (10) with the coefficients,

$$a_1 = \gamma^3\{z^2(z-1)\lambda - z\} + \gamma^2\{z(2z^2 - 2z - 1)\lambda - 2z - 1\}$$
$$+ \gamma\{2z(z^2 - z - 1)\lambda - 2z - 1\} + z\{(z^2 - z - 1)\lambda - 1\},$$

$$a_2 = z\gamma[\gamma^2\{z + 1 - 2z(z-1)\lambda\} + \gamma\{z + 3 - (3z^2 - 4z - 1)\lambda\}$$
$$+ z + 1 - (2z^2 - 3z - 1)\lambda],$$

$$a_3 = z^2\gamma^2[\gamma\{-1 + \lambda(z-1)\} - 1 + \lambda(z-2)]. \quad (B1)$$

The critical curve $\lambda_c(\gamma)$ is given by setting $a_3 = 0$. Only for $\lambda > \lambda_c(\gamma)$ does the quadratic factor of Eq. (10) have a positive root.

## APPENDIX C: THE JACOBIAN OF THE LINEARIZED PA-SIRS

The Jacobian of the linearized PA-SIRS is written

$$\mathbf{A} = \begin{pmatrix} -\gamma & 1 & 0 & 0 & 0 \\ 0 & -1 & z\lambda & 0 & 0 \\ -K_2K_0 & -K_2K_0 & K_3 & -\dfrac{K_1}{\bar{P}(SR)} & \gamma \\ \gamma - K_2 & -K_2 & 1 - \dfrac{K_1}{\bar{P}(IS)} & -2\gamma - \dfrac{K_1}{\bar{P}(SR)} & -\gamma \\ K_2 & 1 + K_2 & -1 + \dfrac{K_1}{\bar{P}(IS)} & \dfrac{K_1}{\bar{P}(SR)} & -\gamma - 2 \end{pmatrix},$$

where

$$K_0 = 1 + 2\frac{\bar{P}(IS)}{\bar{P}(SR)},$$

$$K_1 = \frac{(z-1)\lambda\bar{P}(IS)\bar{P}(SR)}{1 - \bar{P}(R) - \bar{P}(I)},$$

$$K_2 = \frac{(z-1)\lambda\bar{P}(IS)\bar{P}(SR)}{[1 - \bar{P}(R) - \bar{P}(I)]^2},$$

and

$$K_3 = (z-2)\lambda - 1 - K_1\left(\frac{1}{\bar{P}(IS)} + \frac{4}{\bar{P}(SR)}\right).$$

## APPENDIX D: LINEAR STABILITY ANALYSIS OF THE MF-SIRS

The Jacobian matrix B of the linearized MF-SIRS is given by [31]

$$\mathbf{B} = \begin{pmatrix} -\lambda z\bar{P}(I) - \gamma & -\lambda z\bar{P}(S) - \gamma \\ \lambda z\bar{P}(I) & \lambda z\bar{P}(S) - 1 \end{pmatrix}.$$

The characteristic polynomial of the second order, $P_2(\xi) = \xi^2 + a_1\xi + a_2 = 0$, is obtained from $|B - \xi I| = 0$.

The necessary and sufficient (Routh-Hurwitz) conditions [31] for Re $\xi < 0$ are $a_2 > 0$ and $a_1 > 0$. In the coexistence region where $z\lambda > 1$, $a_2 = \gamma(z\lambda - 1) > 0$ and $a_1 = [\gamma/(\gamma+1)] \times (\gamma + z\lambda) > 0$ for all $\gamma > 0$. In the no-coexistence region where $z\lambda < 1$, $a_2 = \gamma(1 - z\lambda) > 0$ and $a_1 = \gamma + (1 - z\lambda) > 0$ for all $\gamma > 0$. Both in the coexistence and no-coexistence region, the real part of the eigenvalues is negative and thus the mean-field steady states are stable.

Now we turn our attention to the oscillatory behavior. The eigenvalues of the characteristic polynomial $P_2(\xi)$ are given by

$$\xi_{\pm} = \frac{-\gamma^2 - z\gamma\lambda \pm \sqrt{[2\gamma z^2 \lambda^2 - 2z\lambda(\gamma^2 + 2z\gamma\lambda + 2) + \gamma^3 + 4\gamma^2 + 8\gamma + 4]\gamma}}{2(\gamma+1)}. \tag{D1}$$

In the range of $\lambda_-(\gamma) < \lambda(\gamma) < \lambda_+(\gamma)$, the imaginary part of the eigenvalues is nonzero,

$$\lambda_{\pm}(\gamma) = \frac{2 + 4\gamma + \gamma^2 \pm 2(1+\gamma)^{3/2}}{z\gamma}.$$

In this range of $\lambda$, the steady states correspond to the stable spiral and the system converges to the steady state in a damped oscillatory pattern. Even in the damped oscillatory region, any oscillation is hardly visible in the large $\gamma$ limit and becomes noticeable only in small $\gamma$ limit.

### APPENDIX E: MONTE CARLO SIMULATION

The numerical simulations described here used lattices with periodic boundary conditions. In one dimension, rings of $5000 \leq N \leq 15\,000$ sites were used. In two dimensions, torii of $50^2 \leq N \leq 200^2$ sites were employed.

To obtain the steady state of the SIRS process, a random initial configuration of susceptible and infected sites is evolved according to the transition rates in Eq. (1). In practice, a site is randomly chosen and a random number ($\in [0,1]$) is also chosen: if it is greater than the given transition probability for that site, which is equal to the rate $\times \Delta t$, its state is updated: $\Delta t$ is chosen to be so small that transition probability is not greater than 1 for a range of $(\lambda, \gamma)$ [8,32]. Otherwise its state remains the same.

For a finite system, the only true stationary state of the SIRS process is the absorbing state corresponding to $P(S)$ $= 1$, $P(I) = P(R) = 0$. To learn about the active state from simulations of a finite system, we study the quasistationary state. These are determined from averages over the surviving representatives of $10^3 - 10^4$ independent realizations of the SIRS process with the same parameter $(\lambda, \gamma)$, beginning with a random initial distribution of the $I$'s. Surviving sample averages converge to stationary values as $N \to \infty$. To obtain the steady states and critical curve, we extrapolated quasistationary values of finite systems to those of the infinite system.

The finite-size scaling theory [8] can be used to obtain the critical curve $\lambda_c^z(\gamma)$. We can assume a scaling function of the surviving probability: $P_t(I) \sim t^{-\beta/\nu_{\parallel}} f[(\lambda - \lambda_c)t^{1/\nu_{\parallel}}]$. At criticality, $\lambda = \lambda_c(\gamma)$, the survival probability of the infection, starting from a single infected site, has a power-law behavior in time. In the subcritical region it decays exponentially, while in the supercritical region it reaches nonzero steady state in a short time. The power-law behavior of the survival probability at criticality enables one to extract the critical curve $\lambda_c^z(\gamma)$ from the time-evolution data of the SIRS process. This dynamical Monte Carlo simulation is reliable when the system size is sufficiently large so that the evolution of the system is approximately confined, for the duration of the simulation to a region smaller than the size of the system [33]. However, we found that this surviving probability oscillates wildly when $\gamma$ is small. Because of this, the dynamical Monte Carlo method is not used to determine the critical curve near $\gamma$ $= 0$.

[1] R. M. Anderson and R. M. May, *Infectious Diseases of Humans: Dynamics and Control* (Oxford University Press, Oxford, 1992).

[2] O. Diekmann and J. A. P. Heesterbeek, *Mathematical Epidemiology of Infectious Diseases: Model Building, Analysis and Interpretation* (Wiley, New York, 2000).

[3] S. M. Krone and C. Neuhauser, J. Appl. Probab. **37**, 1044 (2000).

[4] *Comparative Epidemiology of Plant Diseases*, edited by J. Kranz (Springer-Verlag, New York, 2002).

[5] R. Durrett and S. Levin, Theor Popul. Biol. **28**, 263 (1994).

[6] T. M. Liggett, *Interacting Particle Systems* (Springer-Verlag, New York, 1985).

[7] R. Durrett, *Lecture Notes on Particle Systems and Percolation* (Wadsworth, Pacific Grove, CA, 1988).

[8] J. Marro and R. Dickman, *Nonequilibrium Phase Transitions in Lattice Models* (Cambridge University Press, Cambridge, 1999).

[9] A. De Masi, P. A. Ferrari, and J. L. Lebowitz, Phys. Rev. Lett. **55**, 1947 (1985); J. Stat. Phys. **44**, 589 (1986).

[10] J. L. Lebowitz, Physica A **140**, 232 (1986).

[11] J. L. Lebowitz, E. Presutti, and H. Spohn, J. Stat. Phys. **51**, 841 (1988).

[12] R. Durrett and C. Neuhauser, Ann. Prob. **22**, 289 (1994).

[13] M. Bramson, Ann. Appl. Probab. **7**, 565 (1997).

[14] R. Dickman, Phys. Rev. A **34**, 4246 (1986); **38**, 2588 (1988).

[15] H. Matsuda, N. Ogata, A. Sasaki, and K. Sato, Prog. Theor. Phys. **88**, 1035 (1992).

[16] S. Levin and R. Durrett, Philos. Trans. R. Soc. London, Ser. B **351**, 1615 (1996).

[17] D. ben-Avraham and J. Kohler, Phys. Rev. A **45**, 8358 (1992).

[18] T. Petermann and Paolo De Los Rios, e-print q-bio.PE/0401028.

[19] D. Mollison and S. Levin, in *Ecology of Infectious Diseases in Natural Populations*, edited by B. T. Grenfell and A. P. Dobson (Cambridge University Press, Cambridge, 1995), p. 384.

[20] *Spatial Ecology: The Role of Space in Population Dynamics and Interspecific Interactions*, edited by D. Tilman and P. Kareiva (Princeton University Press, Princeton, 1997).

[21] R. Durrett and S. Levin, Theor Popul. Biol. **53**, 30 (1998).

[22] M. J. Keeling, Proc. R. Soc. London, Ser. B **266**, 859 (1999); **266**, 953 (1999); Ecol. Lett. **5**, 20 (2002).

[23] A. Gandhi, S. Levin, and S. Orszag, Bull. Math. Biol. **62**, 595 (2000).

[24] R. B. Schnazi, Theor Popul. Biol. **61**, 163 (2002).

[25] *The Geometry of Ecological Interactions: Simplifying Spatial Complexity*, edited by U. Diekmann, R. Law, and J. A. Metz (Cambridge University Press, Cambridge, 2000).

[26] J. Van Den Berg, G. Grimmett, and R. Schinazi, Ann. Appl. Probab. **8**, 317 (1998).

[27] E. Andjel and R. Schinazi, J. Appl. Probab. **33**, 741 (1996).

[28] R. Durrett and C. Neuhauser, Ann. Appl. Probab. **1**, 189 (1991).

[29] K. Kuulasmaa, J. Appl. Probab. **25**, 745 (1982).

[30] K. Huang, *Statistical Mechanics* (Wiley, New York, 1987).

[31] J. D. Murray, *Mathematical Biology* (Springer-Verlag, New York, 1980).

[32] R. Durrett and S. Levin, Philos. Trans. R. Soc. London, Ser. B **343**, 329 (1994).

[33] P. Grassberger and A. de la Torre, Ann. Phys. (N.Y.) **122**, 373 (1979).

[34] M. Kobayashi, K. Sato, and N. Konno, Trans. Mater. Res. Soc. Jpn. **26**, 365 (2001).